Chapter 1

Mesoscopic Imaging of Neurotransmitters and Neuromodulators with Genetically Encoded Sensors

Fei Deng, Jiesi Feng, Hao Xie, and Yulong Li

Abstract

Neurotransmitters (NTs) and neuromodulators (NMs) play vital roles in various physiological and pathological processes. To better understand the transmission mechanisms of NTs or NMs (NTs/NMs), it is critical to monitor the dynamics of NTs/NMs with high sensitivity, specificity, and spatiotemporal resolution. With recent advances in genetically encoded NT/NM indicators (GENIs) and mesoscopic imaging, it is now possible to visualize the spatiotemporal dynamics of NTs/NMs in vivo on a large scale, even cover the entire mouse neocortex, enabling simultaneous recording of multiple brain regions to further investigate the relationship among different cortex regions. Here, we present an overview of the principle, development, and application of GENIs, focusing on their joint utilization with mesoscopic imaging.

Key words Neurotransmitter, Neuromodulator, GENI, Sensor, PBP, GPCR, GRAB, Mesoscopic imaging

1 Introduction

As one of the most complex organs in our body, the brain plays essential but diversified functions via interconnected neural networks consisting of billions of neurons and other cells, such as glia. To decipher neural networks, it is critical to monitor neural activities. The recording of neural activities has been revolutionized by advances in voltage and calcium sensors, as discussed in previous chapters, which deepens our understanding of neuromodulation. However, mysteries are still embedded in the nervous system because recording neural activities alone does not capture communications between different cells directly, particularly the molecular dynamics during signal transmission in neural networks.

As we know, neurons communicate with each other via synapses, including electrical synapses and chemical synapses. Chemical synapses, as the predominant synapse, can release and receive neurotransmitters and neuromodulators (NTs/NMs) for

James E. Niemeyer et al. (eds.), *Awake Behaving Mesoscopic Brain Imaging*, Neuromethods, vol. 214,
https://doi.org/10.1007/978-1-0716-4120-0_1,

signal transduction [1]. Typically, NTs/NMs are released from the presynaptic terminal and bind to receptors on the postsynaptic cells, regulating the excitability and gene expression of targeted cells. There are over 100 different NTs/NMs, which can be classified into acetylcholine (ACh), amino acids, monoamines, nucleotides, neuropeptides, and neurolipids [2, 3]. The neurotransmission mediated by NTs/NMs involves many critical physiological processes, such as arousal, attention, appetite, sleep–wake cycles, perception, emotion, reward, learning, and memory [4, 5]. In contrast, the malfunction of neurotransmission is associated with many brain disorders, including depression, addiction, anxiety, epilepsy, schizophrenia, and even Alzheimer's and Parkinson's disease [6–12]. So, there is an urgent need to monitor NTs/NMs with high sensitivity, specificity, and spatiotemporal resolution, which will enhance our comprehension of their functions and may also provide valuable insights into the treatment of related diseases.

Various methodologies have been developed to detect NT/NM dynamics, including traditional methods and newly developed genetically encoded NT/NM indicators (GENIs), which have been extensively reviewed elsewhere [2, 3, 13, 14]. Traditional methods show different limitations, in terms of sensitivity, molecular and cell-type specificity, temporal and spatial resolution, and invasiveness, particularly for in vivo detection. For example, microdialysis has a relatively slow sampling rate, usually about 5–10 min; while fast-scan cyclic voltammetry (FSCV) struggles to distinguish chemicals with similar structures; and electrophysiology requires the application of receptor antagonists to verify molecular specificity. In addition, these three methods are invasive and low-throughput. Although some traditional genetically encoded methods have already been developed, such as SNAP-tag based indicator proteins with a fluorescent intramolecular tether (Snifits [15]), cell-based neurotransmitter fluorescent engineered reporters (CNiFERs [16]), and the TANGO assay [17], they still cannot fulfill the in vivo detection requirements. In contrast, newly developed GENIs offer numerous advantages over traditional methods, including high sensitivity, specificity, and spatiotemporal resolution as well as less invasiveness (Fig. 1). These advantages are especially significant when combined with mesoscopic imaging, which provides a large field of view (FOV) spanning millimeters at video frame rate [18]. According to the Allen brain atlas, there are 43 isocortical areas with distinct functions [19], such as visual, somatosensory, and motor cortex. By simultaneously imaging NT/NM dynamics in different regions under different conditions, we can gain a better understanding of their release patterns and relationships. Moreover, multiple NTs/NMs can be simultaneously monitored with multicolor GENIs in the same cortical region or even same-color GENIs in different regions, benefited from the large FOV of mesoscopic imaging. Overall, GENIs in combination with

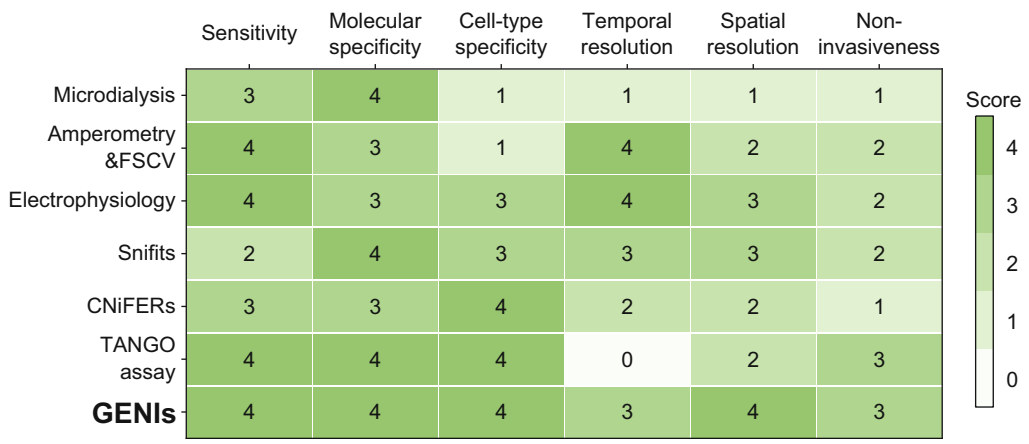

Fig. 1 Current methods for detecting neurotransmitters and neuromodulators. Several current methods are evaluated in different aspects with corresponding scores. The higher score indicates better performance and GENIs exhibit an overall superior performance. FSCV fast-scan cyclic voltammetry, Snifits SNAP-tag based indicator proteins with a fluorescent intramolecular tether, CNiFERs cell-based neurotransmitter fluorescent engineered reporters, GENIs genetically encoded neurotransmitters or neuromodulators indicators

mesoscopic imaging are a powerful technique for investigating the intricate dynamics of NTs/NMs in the brain.

In this chapter, we will introduce GENIs and their fundamental concepts. Additionally, we will discuss how GENIs can be applied in mesoscopic imaging, and provide an example to illustrate the primary workflow.

2 Genetically Encoded Neurotransmitter and Neuromodulator Sensors

Here, we will firstly provide a comprehensive overview of GENIs, including their principles and properties. Next, we will summarize general strategies for developing and optimizing GENIs to meet the requirements for in vivo applications. Lastly, we will discuss different methods for delivering GENIs to animals for whole cortex expression and considerations when using GENIs for mesoscopic imaging.

2.1 Principles and Properties of GENIs

A GENI usually consists of a recognition module and a reporter module, typically connected by linkers (Fig. 2). The recognition module binds the NT/NM molecules and induces conformational changes, which can be transduced to the reporter module to report signal changes by various readouts, such as fluorescence intensity.

So far, two main types of scaffolds have been employed as the recognition module in GENIs, including periplasmic binding proteins (PBPs) and G-protein-coupled receptors (GPCRs). PBPs of gram-negative bacteria belong to a widespread protein superfamily, capable of binding a variety of ligands [20]. Upon ligand binding,

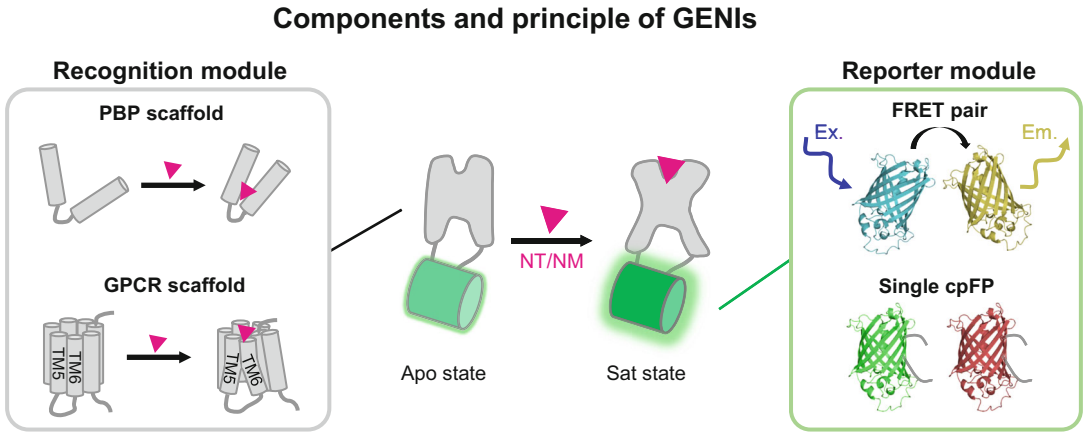

Fig. 2 Components and principle of genetically encoded NT/NM indicators (GENIs). A GENI consists of a recognition module and a reporter module. Upon binding with NT/NM, it can change from the Apo (ligand-free) to Sat (ligand-bound) state, producing changeable fluorescence signals. PBP periplasmic binding protein, GPCR G protein-coupled receptor, FRET fluorescence resonance energy transfer, cpFP circularly permuted fluorescent protein

PBPs change from a ligand-free open state to a ligand-bound closed state, which can transduce large conformational changes to the reporter module. In the past decades, a series of sensors have been developed based on PBPs, such as glutamate [21–24], GABA [25], ATP [26], ACh [27], and serotonin (5-HT) [28] sensors. Another class of recognition modules are GPCRs, which are the most prominent family of membrane receptors and can detect most extracellular signaling molecules, including NTs/NMs [29]. GPCRs share a highly conserved structure, composed of seven transmembrane helices (TM1–TM7), three extracellular loops (ECLs) and three intracellular loops (ICLs), an N-terminal, and a C-terminal. Upon binding its corresponding ligand, the GPCR undergoes a conformational change from an inactive state to an active state, leading to significant structural changes, particularly between TM5 and TM6 [30]. After years of dedicated efforts, many GPCR-based sensors have also been developed, such as ACh [31, 32], dopamine (DA) [33–36], norepinephrine (NE) [37, 38], 5-HT [39–41], adenosine (Ado) [42, 43], adenosine 5′--triphosphate (ATP) [44], and histamine (HA) [45] sensors.

Both PBPs and GPCRs have their own advantages and limitations, including the following:

1. PBP-based sensors can be expressed not only in the cell membrane with some membrane-tethered motifs for detecting extracellular NTs/NMs but also in the cytosol or some organelles for intracellular detections [28]. While most GPCR-based sensors can only localize to cell membrane, which limits their application in intracellular compartments.

2. GPCR-based sensors inherit the pharmacological properties of the endogenous GPCR, which may be a double-edged sword. On the one hand, agonists or antagonists can be used to verify signals of the sensor, serving as an internal control; on the other hand, it is important to avoid using drugs that can directly affect sensor performance when monitoring NTs/NMs in vivo. However, this property can also be leveraged to screen for drugs that can bind to endogenous GPCRs. For example, using a 5-HTR2A-based sensor, PsychLight, Dong et al. successfully identified a non-hallucinogenic psychedelic analog [40]. In contrast, PBP-based sensors are less likely to be affected by some drugs targeting GPCRs since PBPs are derived from bacteria.
3. GPCRs typically have affinities in accord with physiological concentrations, making them more suitable for detecting NTs/NMs in most physiological conditions. Moreover, for some of NTs/NMs, there may be multiple subtypes of GPCRs with varying affinities, which can be developed to sensors with a wide range of affinities. For example, there are 12 subtypes of GPCRs for 5-HT with half-maximal effective concentration (EC_{50}) ranging from nanomolar to micromolar [46], which are appropriate for detecting 5-HT levels both in physiological and pathological conditions [47–49]. Thus, a variety of GPCR-based sensors with different affinities have been developed, with EC_{50} ranging from nanomolar to micromolar [39–41, 50]. And in general, sensors with lower affinities have faster off kinetics, which are more suitable for detecting transients of NTs/NMs. In contrast to GPCR-based sensors, most of PBP-based sensors have low affinities and fast off kinetics.
4. There are limited PBPs that can bind NTs/NMs, which restricts the expansion of PBP-based sensors for most NTs/NMs. It is possible to engineer the binding pocket of an existing PBP to tune its selectivity for other NTs/NMs, as demonstrated in one of the state-of-the-art works that a 5-HT sensor, iSeroSnFR, was redesigned from an ACh sensor, iAChSnFR [28]. However, its sensitivity is still not satisfied for in vivo detection of 5-HT dynamics. Moreover, it is quite difficult and laborious to expand this strategy to other NT/NMs for developing highly selective sensors. In contrast, for most NTs/NMs, there is at least one endogenous GPCR that can bind to NTs/NMs, making it more practical to develop GPCR-based sensors for most NTs/NMs.

The reporter module can be used to transduce conformational changes of the recognition module into various signals, and fluorescence is one of the most commonly used signals. This can be

achieved by either a fluorescence resonance energy transfer (FRET) pair or a single fluorescent protein (FP). The reporter module of a FRET-based sensor consists of a FRET pair with both a donor and an acceptor fluorescent protein, such as CFP and YFP [51]. The conformational changes in the recognition module can alter the distance and orientation between the FRET pair, thereby modulating the FRET efficiency and leading to changes in the fluorescent intensity ratio between the donor and acceptor. FRET-based sensors can be used as ratiometric sensors since they rely on two spectral-distinct FPs, making them resistant to artifacts (e.g., movement), and suitable for analyte quantification. However, FRET-based sensors have limited dynamic range due to the steric hindrance of the bulky FP moiety, which prevents the FRET pair from getting close enough to each other. For example, a FRET-based 5-HT sensor, named 5HT-CC, exhibited good membrane localization and high selectivity to 5-HT, but only a ~4% increase in FRET ratio in response to saturated 5-HT [52]. Nonetheless, no in vivo application of 5HT-CC has been reported yet, possibly due to its insufficient sensitivity. Single FP-based sensors typically contain a circularly permuted FP (cpFP) or split FP, and their fluorescence intensities change with the conformational changes of the recognition module. And a circularly permutated enhanced green fluorescent protein (cpEGFP) is widely used in most single FP-based sensors. Unlike FRET sensors, their dynamic ranges are not limited by the FRET efficiency and can show relatively high response, making them suitable for in vivo applications. For example, a green fluorescent 5-HT sensor, named $GRAB_{5\text{-}HT1.0}$, can report endogenous 5-HT release in flies and mice with over 50% fluorescence increases evoked by odor and MDMA application, respectively [39]. Most single FP-based sensors are intensiometric, with one excitation or emission peak. Thus, these intensiometric sensors are also suitable for commonly used and low-cost imaging systems, such as the fiber photometry recording system.

Considering that single FP-based sensors show good performance and have been used in vivo, properties for most GENIs with single chromophore are summarized in Table 1.

2.2 Development and Optimization of GENIs

As mentioned above, GENIs consist of a recognition module, a reporter module, and linkers. To develop a GENI, the first step is to screen a well-performed recognition module and an appropriate reporter module. Then, the best insertion site for the reporter module should be scanned and some critical residues of the sensor can be further optimized. The detailed workflow has been summarized in other reviews using DA sensors as examples [2, 3, 53]. Using native GPCR as the recognition module, a series of GENIs have been developed recently.

Here, we take the $GRAB_{5\text{-}HT}$ sensor [39] (GRAB stands for GPCR activation-based) as an example to illustrate the typical

Table 1
Summary of single FP-based GENIs

NTs/NMs types	Sensor name	Recognition module	Reporter module	Ex/Em (nm)	Responses (max. $\Delta F/F_0$)	Affinity (EC50)	In vivo application	Refs.
Amino acids	*Glutamate sensors*							
	iGluSnFR3.v82	*E. coli* GltI	cpmVenus	512/530	13.1[a]	31.7 μM[a]	Mouse	[90]
	iGluSnFR3.v857	*E. coli* GltI	cpmVenus	502/522	54.0[a]	195.9 μM[a]	Mouse	[90]
	SF-iGluSnFR. A184S	*E. coli* GltI	cpsfGFP	490/510	3.1[a]/0.69[b]	7.5 μM[a]	Mouse, ferret	[23]
	$iGlu_u$	*E. coli* GltI	cpEGFP	NA	2.8[a]/1.7?[b]	600 μM[a]/53 μM[b]	NA	[91]
	R-iGluSnFR1	*E. coli* GltI	cpmApple	562/588	-4.9[a]/−0.35[b]	11 μM[a]	NA	[24]
	GABA sensors							
	iGABASnFR	Pf622	cpsfGFP	485/510	2.5[a]/~0.7[b]	9 μM[a]/30 μM[b]	Mouse	[25]
	iGABASnFR. F102G	Pf622	cpsfGFP	NA	4.5[a]/~1.7[b]	50 μM[a]/42 μM[b]	Mouse	[25]
	iGABASnFR. F102Y.Y137L	Pf622	cpsfGFP	NA	3.5[a]/~0.45[b]	70 μM[a]/106 μM[b]	Mouse, zebrafish	[25]
Acetylcholine	*Acetylcholine sensors*							
	$GRAB_{ACh3.0}$	M_3R	cpEGFP	492/510	2.8[b]/~2.7[c]	2.2 μM[c]	Mouse, fly	[32]
	iAChSnFR	X513-OpuBC	cpsfGFP	485/510	12[a]/10[b]/~4.5[c]	1.3 μM[a]/2.9 μM[b]/0.4 μM[c]	Mouse, zebrafish, fly, worm	[27]
Monoamines	*Dopamine sensors*							
	$GRAB_{DA2h}$	D_2R	cpEGFP	500/520	~2.8[b]/~2.4[c]	7 nM[b]/28 nM[c]	Mouse	[34]
	$GRAB_{DA2m}$	D_2R	cpEGFP	NA	~3.4[b]/~3.1[c]	90 nM[b]/104 nM[c]	Mouse, fly	[34]
	$rGRAB_{DA1h}$	D_2R	cpmApple	565/595	~1.0[b,c]	4 nM[b]/18 nM[c]	Mouse	[34]
	$rGRAB_{DA1m}$	D_2R	cpmApple	565/595	~1.5[b]/~1.7[c]	95 nM[b]/ 93 nM[c]	Mouse, fly	[34]
	dLight1.1	D_1R	cpEGFP	490/516	2.3[b]	330 nM[b]	Mouse	[35]
	dLight1.2	D_1R	cpEGFP	490/516	3.4[b]	770 nM[b]	Mouse	[35]
	dLight1.3b	D_1R	cpEGFP	NA	9.3[b]	1680 nM[b]	Mouse, rat	[14, 35]
	dLight1.4	D_4R	cpEGFP	NA	1.7[b]	4.1 nM[b]	NA	[35]
	dLight1.5	D_2R	cpEGFP	NA	1.8[b]	110 nM[b]	NA	[35]
	YdLight1	D_1R	cpEGFP	NA/525	3.06[b]	1.63 μM[b]	NA	[36]

(continued)

Table 1
(continued)

NTs/NMs types	Sensor name	Recognition module	Reporter module	Ex/Em (nm)	Responses (max. $\Delta F/F_0$)	Affinity (EC50)	In vivo application	Refs.
	RdLight1	D_1R	cpmApple	562/588	2.48[b]/~3[c]	859 nM[b]/ 229 nM[c]	Mouse, rat	[36]
	R-GenGAR-DA1.2	D_1R	cpmApple	566/595	-0.43[b]/−0.52[c]	920 nM[b]/250 nM[c]	NA	[92]
	Noradrenaline sensors							
	$GRAB_{NE1h}$	$\alpha_{2A}R$	cpEGFP	NA	1.3[b]/1.5[c]	83 nM[b]/ 229 nM[c]	Mouse, zebrafish	[37]
	$GRAB_{NE1m}$	$\alpha_{2A}R$	cpEGFP	NA	2.3[b,c]	930 nM[b]/ 229 nM[c]	Mouse, zebrafish	[37]
	nLight1.3	$\beta_{2A}R$	cpEGFP	NA/516	~2.1[b]/1.3[c]	764 nM[b]/ 919 nM[c]	Mouse	[38]
	Serotonin sensors							
	iSeroSnFR	X513-OpuBC	cpsfGFP	NA	8[a]/17[b,c]	310 μM[a]/390 μM[b]	Mouse	[28]
	$GRAB_{5\text{-}HT1.0}$	$5\text{-}HT_{2C}R$	cpEGFP	NA	2.5[b]/2.8[c]	14 nM[b]/ 22 nM[c]	Mouse, fly	[39]
	PsychLight2	$5\text{-}HT_{2A}R$	cpEGFP	NA	0.8[c]	26 nM[c]	Mouse	[40]
	$GRAB_{HTR6\_1.0}$	$5\text{-}HT_6R$	cpEGFP	NA	1.5[b]	84 nM[b]	NA	[93]
	sDarken	$5\text{-}HT_{1A}R$	cpEGFP	NA	-0.71[b]	127 nM[b]	Mouse	[41]
	$gGRAB_{5\text{-}HT3.0}$	$5\text{-}HT_4R$	cpEGFP	505/520	13[b]/27[c]	150 nM[b]/ 80 nM[c]	Mouse	[50]
	$rGRAB_{5\text{-}HT1.0}$	$5\text{-}HT_4R$	cpmApple	560/595	3.3[b]/4[c]	790 nM[b]/ 600 nM[c]	Mouse	[50]
	Histamine sensors							
	$GRAB_{HA1h}$	hH_4R	cpEGFP	505/520	3.7[b]/1.8[c]	17 nM[b]/ 19 nM[c]	Mouse	[45]
	$GRAB_{HA1m}$	wbH_1R	cpEGFP	505/520	5.9[b]/3.2[c]	380 nM[b]/ 400 nM[c]	Mouse	[45]
Nucleotides	*Adenosine sensors*							
	$GRAB_{Ado1.0}$	$A_{2A}R$	cpEGFP	NA	1.2[b]/2[c]	60 nM[c]	Mouse	[42, 43]
	$GRAB_{Ado1m}$	$A_{2A}R$	cpEGFP	NA	3.5[c]	3.6 μM[c]	Mouse	[42, 43]
	ATP sensors							
	iATPSnFR1.0	F_0F_1-ATP synthase ε subunit	cpsfGFP	490/512	~2.4[a]/1.0[b]/1.1[c]	~120 μM[a]/350 μM[b]/400 μM[c]	NA	[26]
	ATPOS	F_0F_1-ATP synthase ε subunit	Cy3	556/565	~1.8[a]/1.0[b]/1.1[c]	~150 nM[a]/350 μM[b]/400 μM[c]	Mouse	[94]
	$GRAB_{ATP1.0}$	$hP2Y_1$	cpEGFP	500/520	5[b]/7.8[c]	~6.7 μM[b]/77 nM[c]	Mouse, zebrafish	[44]
	$GRAB_{ATP1.0\text{-}L}$	$hP2Y_1$	cpEGFP	NA	~10[c]	97 μM[b]/32 μM[c]	Zebrafish	[44]

Neuropeptides	*Opioid sensors*							
	kLight1.2a	KOR	cpEGFP	NA	0.6[b]	NA	Mouse	[35, 95]
	GrpLight1.3ER	GRPR	cpEGFP	NA	~8[c]	198 nM[c]	Mouse	[96]
	M-SPOTIT	MOR	cpGFP	NA	12.5[b]/4.6[c]	15 nM[c]	NA	[97]
	Orexin sensor							
	OxLight1	OX_2R	cpEGFP	490/512	9.06[b] (orexin-A), 8.59[b] (orexin-B)	75 nM[b]/127 nM[c] (orexin-A), 47 nM[b]/110 nM[c] (orexin-B)	Mouse	[98]
	Oxytocin sensors							
	$MTRIA_{OT}$	meOTR	cpGFP	NA	7.35[b]	~20 nM[b,c]	Mouse	[99]
	$GRAB_{OT1.0}$	bOTR	cpEGFP	505/520	~4[b]/4.5[c]	1.6 nM[b]/3 nM[c]	Mouse	[100]
	Corticotropin-releasing factor sensor							
	$GRAB_{CRF1.0}$	CRF1R	cpEGFP	500/520	15.6[b]/13.3[c]	33 nM[b]/18 nM[c]	Mouse	[101]
	Somatostatin sensor							
	$GRAB_{SST1.0}$	SSTR5	cpEGFP	500/520	4.2[b]/4.5[c]	70 nM[b]/130 nM[c] (SST-14), 13 nM[b] (SST-28)	Mouse	[101]
	Cholecystokinin sensor							
	$GRAB_{CCK1.0}$	CCKBR	cpEGFP	505/520	7.3[b]/9[c]	4 nM[b]/5.5 nM[c]	Mouse	[101]
	Neurotensin sensor							
	$GRAB_{NTS1.0}$	NTSR1	cpEGFP	NA	3.8[b]	6 nM[b]	NA	[101]
	Neuropeptide Y sensor							
	$GRAB_{NPY1.0}$	NPY1R	cpEGFP	500/520	3[b]	40 nM[b]/0.7 nM[c]	NA	[101]
	Substance P sensor							
	$GRAB_{SP1.0}$	TACR1	cpEGFP	NA	0.7[b]	NA	NA	[101]
	Urocortin sensor							
	$GRAB_{UCN1.0}$	CRF2R	cpEGFP	NA	11.9[b]	NA	NA	[101]
	Vasoactive intestinal peptide sensor							
	$GRAB_{VIP1.0}$	VIPR2	cpEGFP	500/520	4.9[b]	120 nM[b]/19 nM[c]	NA	[101]
	Parathyroid hormone-related peptide sensor							
	$GRAB_{PTH1.0}$	PTH1R	cpEGFP	NA	3.8[b]	NA	NA	[101]
	Glucagon-like peptide-1 sensor							
	GLPLight1	GLP1R	cpEGFP	500/512	5.3[b]/4.6[c]	28 nM[b]/9.3 nM[c]	NA	[102]
Neurolipids	*Endocannabinoid sensor*							
	$GRAB_{eCB2.0}$	CB1R	cpEGFP	500/520	3.3[b]//9.5[c] (2-AG), 2.8[b]/5[c] (AEA)	3.1 μM[b]//9.0 μM[c] (to 2-AG), 0.2 μM[b]/0.8 μM[c] (to AEA)	Mouse	[67]

NA data not available
[a]Measured in purified proteins
[b]Measured in cell lines
[c]Measured in cultured neurons

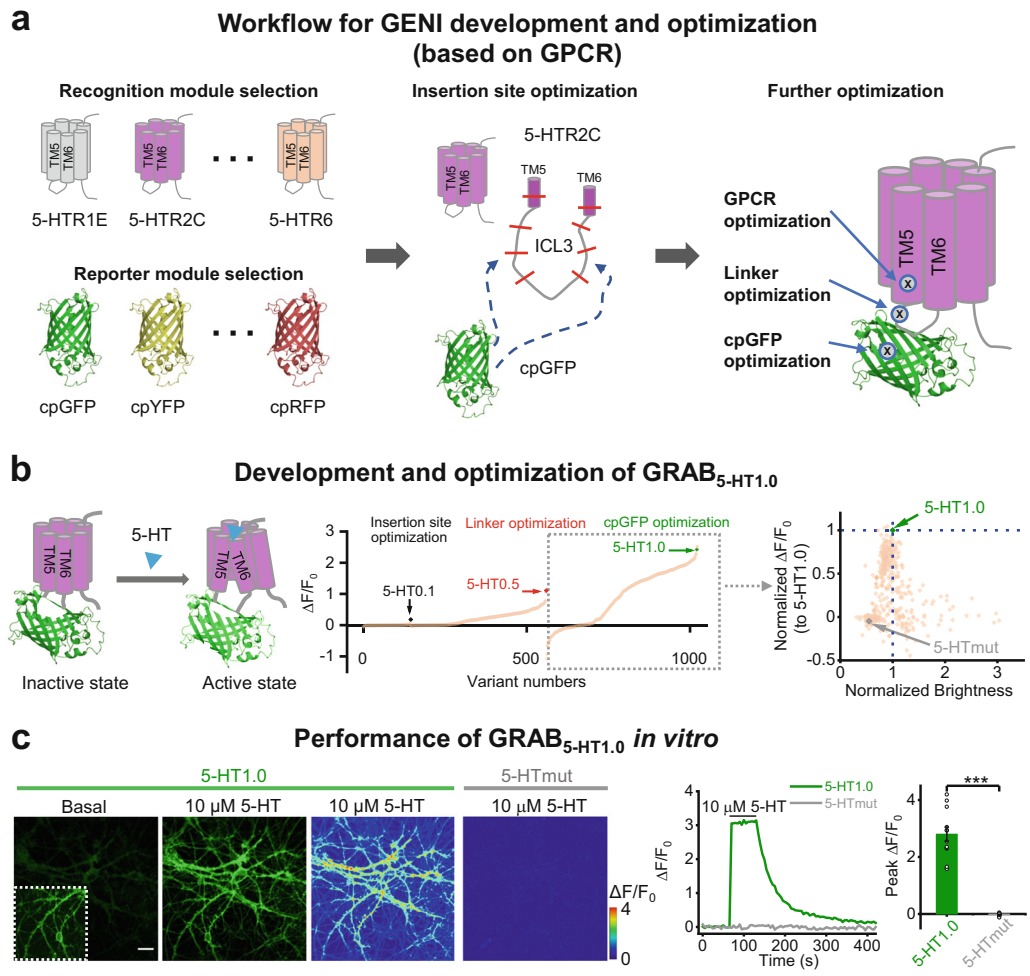

Fig. 3 Development and optimization of genetically encoded NT/NM indicators (GENIs). (**a**) Schematic diagram depicting the general workflow for GENI development and optimization based on GPCR scaffolds, taking the $GRAB_{5\text{-}HT1.0}$ sensor as an example. (**b**) Development and optimization of $GRAB_{5\text{-}HT1.0}$ (adapted from Wan et al. [39]). (**c**) Performance of $GRAB_{5\text{-}HT1.0}$ in cultured rat cortical neurons (adapted from Wan et al. [39]). TM5/TM6 transmembrane domains 5/6, ICL3 the third intracellular loop, cpGFP/cpYFP/cpRFP circularly permuted green/yellow/red fluorescent protein

workflow for developing and optimizing GENIs based on GPCR scaffolds in details (Fig. 3a, b). To choose a suitable GPCR scaffold as the recognition module (*see* **Note 1**), several 5-HT receptor subtypes have been fused with a cpEGFP, examining based on the membrane trafficking and affinities. The 5-HTR2C-based sensors showed the best membrane trafficking and was selected as the scaffold. To better transduce the GPCR conformational changes into the cpEGFP, insertion sites for cpEGFP and linkers were systematically screened. Since the N- and C-terminal linkers between GPCR and cpEGFP are critical for the efficiency of

conformational transduction, linkers have been optimized by site-directed random mutagenesis (*see* **Note 2**). In addition, some sites in cpEGFP, which are contributed to fast GFP folding and high brightness [54, 55], have been optimized as well. After the above rounds of iterative optimization, the finalized best candidate was named the $GRAB_{5\text{-}HT1.0}$ sensor, which showed a ~280% increase in fluorescence ($\Delta F/F_0$) with saturated concentration of 5-HT application. Additionally, a 5-HT-insensitive sensor was generated by introducing the $D134^{3.32}Q$ substitution, which serves as a negative control (Fig. 3b). The $GRAB_{5\text{-}HT1.0}$ sensor also showed good membrane localization and large response in cultured neurons (Fig. 3c).

2.3 Expression of GENIs In Vivo

To deliver GENIs in the mammalian system for in vivo application, two approaches are commonly used, including viral-mediated gene delivery and GENIs knock-in animals.

Viral-mediated gene delivery is a convenient, fast, and versatile approach to achieve efficient expression of GENIs. One of the most popular viral tools is the recombinant adeno-associated virus (rAAV), which is modified from the wild-type AAV, a member of the nonpathogenic parvovirus [56–58]. GENIs can be expressed in specific cell types with different serotypes or promoters, i.e., using the AAV2/9 pseudotype and CaM kinase II alpha (CaMKIIα) promoter to drive GENIs expression in excitatory neurons. Local injections of AAVs are commonly used to achieve regional expression of GENIs in the brain, but global expression in the animal's brain for mesoscopic imaging requires multiple injections due to the limited diffusing distance [58]. Although multiple-site injections in the brain can drive robust expression of GENIs, it is laborious, time-consuming, and hard to make a relatively uniform expression of sensors (*see* **Note 3**). By engineering AAV capsids, some AAV pseudotypes, can efficiently cross the blood-brain barrier and infect the central nervous systems, such as PHP.eB, which can infect more than half of cortical and striatal neurons by intravenous administration [59]. PHP.eB-mediated expression of a calcium sensor, GCaMP6s, works well in mesoscopic imaging [60], but no PHP.eB-mediated expression of GENIs has been reported yet, possibly due to the low expression level and signal-to-noise ratio (SNR). Given that the AAV9 has a capacity to cross the blood-brain barrier (BBB) of mice, especially in neonate [61], a novel method called neonatal sinus injection (short for n-SIM) has been reported recently, which employs transverse sinus injections of AAV9 at P0 pups to efficiently deliver gene across the central nervous system, leading to the whole-brain expression [62]. The n-SIM is suitable for expressing GENIs in animals for mesoscopic imaging, as demonstrated in a study using an acetylcholine (ACh) sensor, $GRAB_{ACh3.0}$, to monitor ACh dynamics in mice across the neocortex [63].

Another approach to driving the expression of GENIs is generating GENI knock-in animals. Compared with viral-mediated expression, transgenic methods expand the ability to monitor and manipulate neuronal activities with increased cell-type specificity and express gene cassettes with larger sizes. Transgenic animals also enable a uniform expression of GENIs in the entire dorsal neocortex, making them ideal for mesoscopic imaging. By genetic manipulation, some GENIs knock-in animals have been developed and are usually in a recombinase-dependent manner, such as the iGluSnFR knock-in mice [64], a fluorescent glutamate sensor line, which has also been successfully used in mesoscopic imaging [65]. With the development of gene editing tools [66] and advancements in the development of a series of GENIs [31–37, 39, 44, 67], it is possible to generate transgenic animals for expression of various GENIs. By crossing with different driver lines, we are also able to express GENIs in specific cells for monitoring NTs/NMs. For example, Feng et al. measured cell type-specific NE signals in response to tactile stimuli by expressing the GRAB$_{NE2m}$ sensor in excitatory neurons or astrocytes via crossing the GRAB$_{NE2m}$ knock-in mice with CaMKIIα-Cre or GFAP-Cre mice, respectively [68]. Although GENI knock-in animals exhibit many advantages, compared with viral-mediated expression, generation of these animals is time-consuming and relatively expensive.

2.4 Considerations for Using GENIs

With the advances in GENIs, a variety of NTs/NMs can be imaged in vitro or in vivo. These sensors have their own advantages but also some limitations. Thus, for the applications of GENIs, especially in vivo, it is important to carefully choose the most appropriate sensor for the specific scenario since there is almost no "one-size-fits-all" sensor [3, 14, 69].

The first thing that needs to be considered is the sensitivity, which is determined by multiple factors including the response, affinity, and brightness, and can be evaluated by signal-to-noise ratio (SNR) [3]. For example, compared with dLight1.3b, although GRAB$_{DA2m}$ has a smaller maximum response (GRAB$_{DA2m}$: ~220%, dLight1.3b: ~450%), it shows a higher SNR (~2-fold to dLight1.3b) owing to higher basal and maximum brightness in HEK293T cells [34]. Importantly, for in vivo application, effective sensitivity is also affected by the resting ligand concentration [2]. So, selecting a sensor with an appropriate affinity for detecting NT/NM levels is crucial to maximize its sensitivity, especially when the sensor's EC_{50} matches the basal ligand concentration.

Another important consideration is the specificity. Although most of GENIs show high specificity to corresponding ligands, some of them also respond to other molecules with similar structures. For example, the excellent sensor engineering leads to an ACh sensor, iAChSnFR, whose specificity is shifted from choline

toward ACh with ~35-fold selectivity but still responds to choline when the concentration of choline is higher than 1 μM [27]. Since ACh released in synapses can be rapidly hydrolyzed to choline by acetylcholinesterase (AChE) [70], which may disturb the interpretation of signals from iAChSnFR. In contrast, the GPCR-based sensor, $GRAB_{ACh}$, does not respond to choline in high concentration even at 100 μM, showing a much more specific response to ACh [31, 32]. Another case is the DA sensor: although GPCR-based DA sensors, including $GRAB_{DA}$ and dLight, have a higher selectivity for DA over NE (~15-fold for $GRAB_{DA2m}$ and ~60-fold for dLight1), they still respond to NE when the NE concentration is higher than 0.1 μM for $GRAB_{DA2m}$ and 1 μM for dLight1, respectively [33–36]. So, it is important to be careful when choosing GENIs and interpreting signals of GENIs that may respond to other molecules.

Third, when selecting GENIs for a specific application scenario, it is important to consider the kinetics of the sensor. For capturing rapid transients of NTs/NMs, GENIs with fast kinetics are needed. However, there is always a tradeoff between a sensor's affinity and off kinetics. That is to say, sensors with fast off kinetics may have a low affinity, which may limit their sensitivities. If fast kinetics are not necessary, GENIs with slow off kinetics but high affinity could also be beneficial, since they accumulate more photons and contribute to higher SNR [39].

Fourth, different pharmacological properties of GENIs should be considered, especially for GPCR-based sensors since most of them inherit the pharmacological properties of parent GPCRs. On the one hand, agonists or antagonists can be used to manipulate sensor signals for validation. On the other hand, it is important to avoid using compounds that interact with sensors when recording the signals of endogenous NTs/NMs. Fortunately, the problem can be circumvented by developing different subtype-based sensors. For example, DA sensor $GRAB_{DA}$ and dLight are based on D_2R and D_1R, respectively.

Last but not least, the expression of GENIs should not affect cell physiology, especially for long-term expression. For GPCR-based sensors, one potential concern is that they may couple with downstream pathways, including G protein and β-arrestin pathways. Fortunately, most GPCR-based sensors have shown negligible downstream signaling, possibly due to the steric hindrance of the bulky cpFP that replaces the ICL3 of the GPCR, which precludes the interaction between the GPCR and G protein or β-arrestin [44]. However, a few GPCR-based sensors still, to some extent, coupled with downstream signaling, such as the $GRAB_{ACh2.0}$ sensor [31]. But this G_q protein coupling was almost eliminated in an optimized version, the $GRAB_{ACh3.0}$ sensor [32]. In addition, overexpression of GENIs may cause potential buffering effects, which may compete with endogenous GPCRs

and affect cell physiology. It is worth noting that current results indicate no obvious buffering effects both in vitro and in vivo [34, 39]. Nevertheless, it is advisable to use more sensitive sensors (higher SNR) with lower affinity and reduce expression levels to minimize the potential buffering effects.

3 Mesoscopic Imaging with GENIs

NTs/NMs are widely distributed throughout the brain and play important roles, such as reward, emotion, learning, and memory. For example, acetylcholine (ACh) and monoamines are very vital NTs/NMs that involve almost all the brain functions and are produced by different neurons. These neurons project to and innervate the entire cortex, which consists of dozens of brain regions (Fig. 4a), according to the Allen CCFv3 atlas [71]. GENIs provide a powerful toolbox for high spatiotemporal imaging of a variety of NTs/NMs. Traditional microscopy, such as

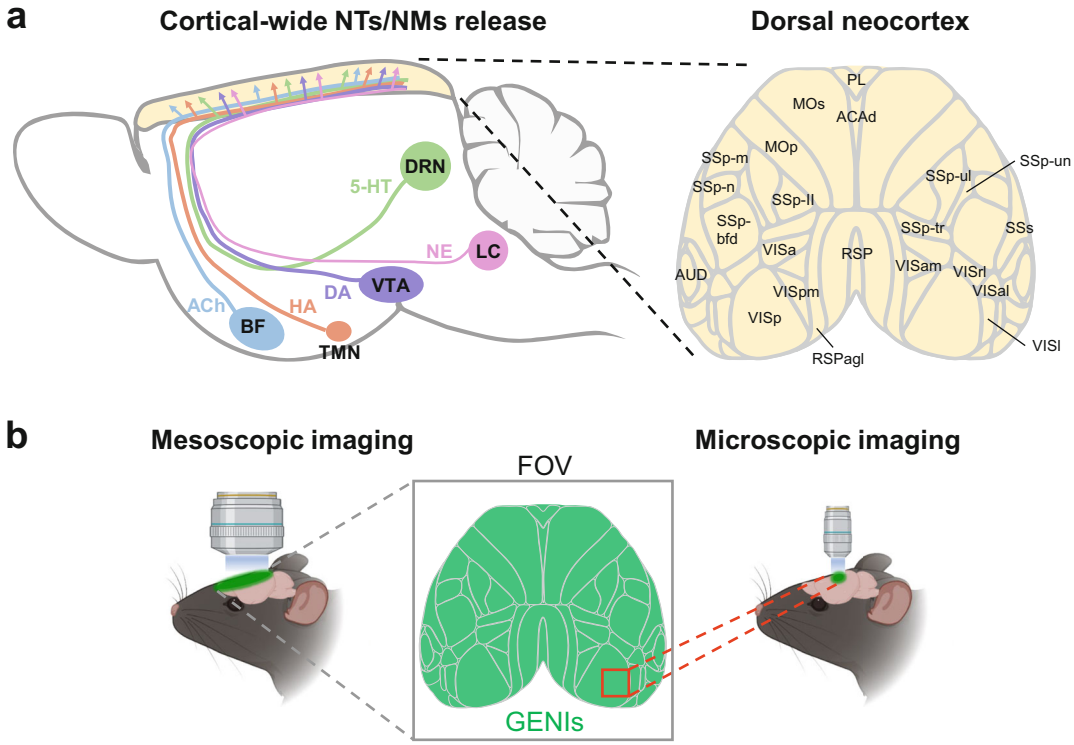

Fig. 4 Combination of mesoscopic imaging and GENIs. (**a**) Schematic diagram depicting the projection of different monoaminergic neurons in the cortex (left) and parcellation of cortical areas (right). (**b**) Comparison of the FOV (field of view) between mesoscopic imaging and microscopic imaging. The black square indicates FOV for mesoscopic microscope; the red square indicates FOV for traditional microscope. BF basal forebrain, DRN dorsal raphe nucleus, LC locus coeruleus, VTA ventral tegmental area, TMN tuberomammillary nucleus

confocal and two-photon microscopes, can provide cellular and subcellular resolution but often with a limited FOV of several hundred microns [18], in which it is hard to monitor the global spatial dynamics of NTs/NMs. Simultaneously imaging NTs/NMs across multiple brain regions can enhance the understanding of NT/NM dynamics and functions in the brain. Mesoscopic imaging, which spans a FOV larger than 1 cm × 1 cm and covers the entire dorsal neocortex of the mouse, offers a powerful tool for large-scale imaging (Fig. 4b).

The combination of GENIs and mesoscopic imaging has greatly facilitated the understanding of NT/NM dynamics, which can lead to new biological discoveries and ideas. Here, we will show some examples of mesoscopic imaging with GENIs.

The earliest mesoscopic imaging with GENIs may be traced back to the mesoscopic imaging of iGluSnFR [65]. Xie et al. expressed iGluSnFR in mouse cortex by AAV injection or transgenic mice and visualized glutamate dynamics with mesoscopic imaging. They detected glutamate release in specific brain regions evoked by multiple sensory stimuli in anesthetized and behaving mice. Moreover, the kinetics of glutamate release reported by iGluSnFR are comparable to signals detected by voltage-sensitive dye (VSD) and much faster than calcium signals reported by GCaMP3 and GCaMP6s. Moreover, using a miniaturized head-mounted microscope, Rynes et al. monitored glutamate dynamics in freely moving mice during the sleep–wake cycle [72].

In addition, it is also important and feasible to detect two different neurochemicals simultaneously with dual-color mesoscopic imaging (*see* **Note 4**). Lohani et al. co-expressed the green fluorescent ACh sensor $GRAB_{ACh3.0}$ and the red fluorescent calcium sensor jRCaMP1b in the mouse dorsal neocortex to simultaneously monitor cholinergic signaling and cortical activity [63]. They found that the ACh signal in the neocortex is highly dynamic and spatially heterogeneous, which can link behavioral fluctuations to the functional reorganization of cortical networks.

Although the combination of mesoscopic imaging with GENIs is a powerful tool for understanding NT/NM dynamics, there are still some limitations and challenges. Firstly, the preparation for animals expressing GENIs uniformly (*see* **Note 3**) may be a rate-limiting step, since n-SIM and crossing of transgenic mice cost more than 6 weeks from the AAV injection or mice crossing, which is much slower than traditional local AAV injection that takes about 3 weeks for expression. Secondly, there are potential signal contaminations from hemodynamic changes [73, 74] and light scattering. For hemodynamic artifacts, if it is not negligible, hemodynamic correction is needed (*see* **Note 5**). In general, there are two correction strategies [18] based on a reference channel. One is using the isosbestic point of the GENI to correct the standard wavelength excited signal. Another is using a reflectance

of green (~530 nm) and red (~630 nm) illumination to measure the hemodynamic changes for correction [18, 73]. Thirdly, most mesoscopic imaging systems are custom-built, which limits the availability of mesoscopic imaging with GENIs for more laboratories. Fortunately, with the generous sharing of imaging system building experience [75] and GENIs, it will be easier for more laboratories to adopt mesoscopic imaging with GENIs for more biological discoveries. Fourthly, signals acquired by mesoscopic imaging are limited in the surface of the sample, which indicates that it is mainly used for imaging the dorsal cortex instead of other deep brain regions. In addition, even in the dorsal cortex, signals from the superficial layer are dominant, which may lead to some bias across different layers.

Despite these challenges, mesoscopic imaging with GENIs can monitor the dynamics of NTs/NMs on a large scale and may provide new insights into their important roles in the nervous system.

4 Case Study: Mesoscopic Imaging of Cortical 5-HT Dynamics in Mouse

Here, an optimized green fluorescent 5-HT sensor, named $gGRAB_{5\text{-}HT3.0}$ (referred to hereafter as simply g5-HT3.0 [50]), is used as an example to demonstrate the monitoring of NT/NM dynamics by mesoscopic imaging.

5-HT is a crucial monoamine that regulates lots of essential biological processes, such as appetite, sleep–wake cycles, emotion, reward, learning and memory [76–78]. Meanwhile, the malfunction of the serotonergic system is associated with many psychiatric disorders, including anxiety, addiction, and depression [6–8]. Moreover, some psychotropic drugs targeting the serotonergic system are widely used to treat brain disorders, e.g., some selective serotonin reuptake inhibitors (SSRIs) are used as antidepressants by inhibiting the reuptake of 5-HT and elevating the extracellular 5-HT level. So, monitoring the dynamics of 5-HT is critical for understanding the serotonergic system. Combining the 5-HT sensor with mesoscopic imaging, there is a great opportunity to visualize the spatiotemporal dynamics of 5-HT across multiple brain regions [79, 80] in real-time.

Since the dorsal raphe nucleus (DRN) is the primary source of serotonergic neurons [81], a Cre-dependent red-shifted optogenetic actuator, ChrimsonR [82], was expressed in the DRN of *Sert-Cre* mice [83] to optically activate serotonergic neurons for 5-HT release to validate the sensor's reliability. Besides artificially evoked 5-HT release in the cortex, considering the important role of 5-HT in regulating sleep–wake cycles [39, 84], the physiological 5-HT dynamics were monitored during sleep–wake cycles using mesoscopic imaging, while simultaneous electroencephalography (EEG)

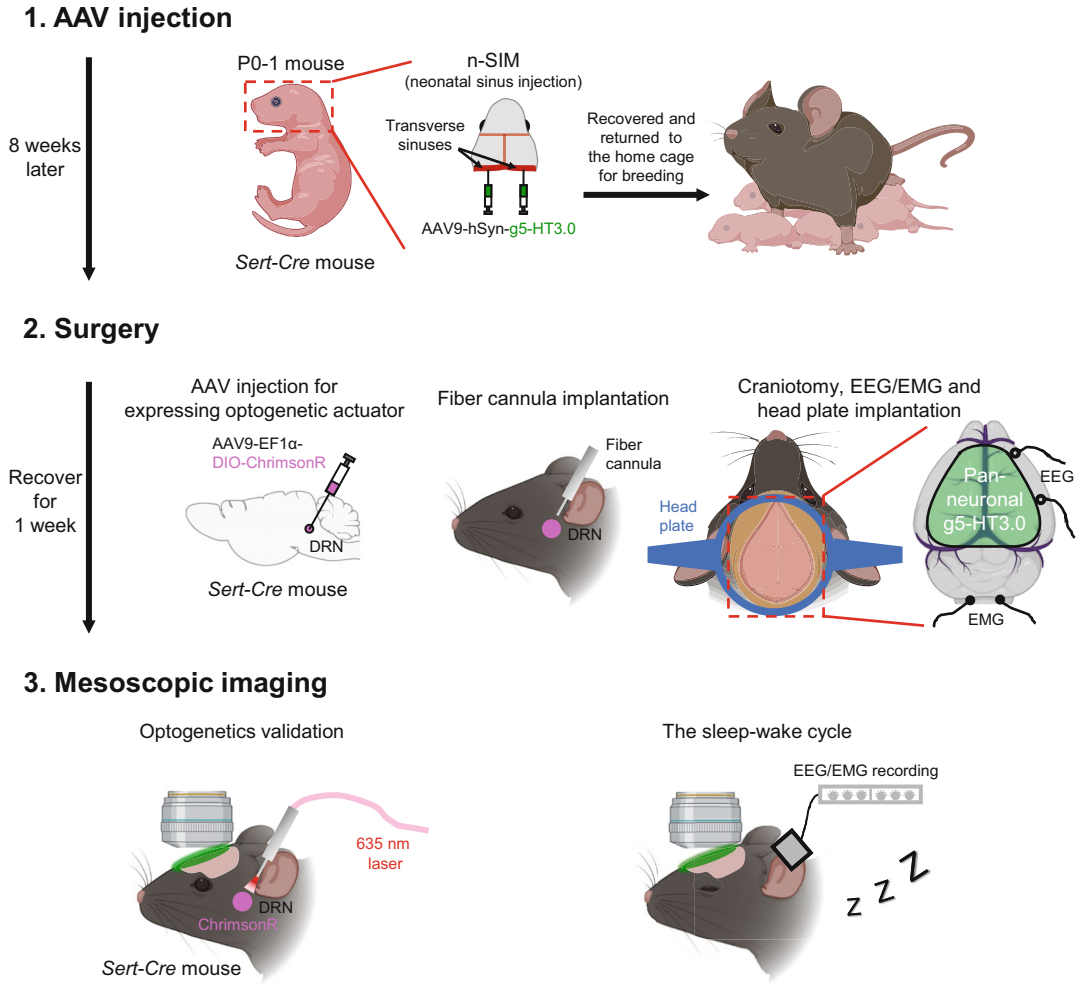

Fig. 5 Workflow of mesoscopic imaging with g5-HT3.0 sensor during optical stimulation of DRN and sleep–wake cycles. Typical workflow for preparing mice for mesoscopic imaging with GENIs, using g5-HT3.0 sensor as an example

and electromyography (EMG) recordings were performed to identify the sleep–wake state of mice.

The example workflow for mesoscopic imaging with a g5-HT3.0 sensor includes three main steps (Fig. 5). The first step involves AAV injection for expressing GENIs. To achieve uniform expression of the sensor, AAVs were injected using the n-SIM method [62] as described above. About 8 weeks later, the second step was performed—the surgery is applied to mice injected with AAVs expressing the g5-HT3.0 sensor. In order to optically activate serotonergic neurons in DRN, AAV (AAV9-EF1a-DIO-ChrimsonR) was injected into the DRN of *Sert-Cre* mice, and an optical fiber cannula was inserted for the delivery of light. Then a large craniotomy was made above the dorsal cortex to create an optical

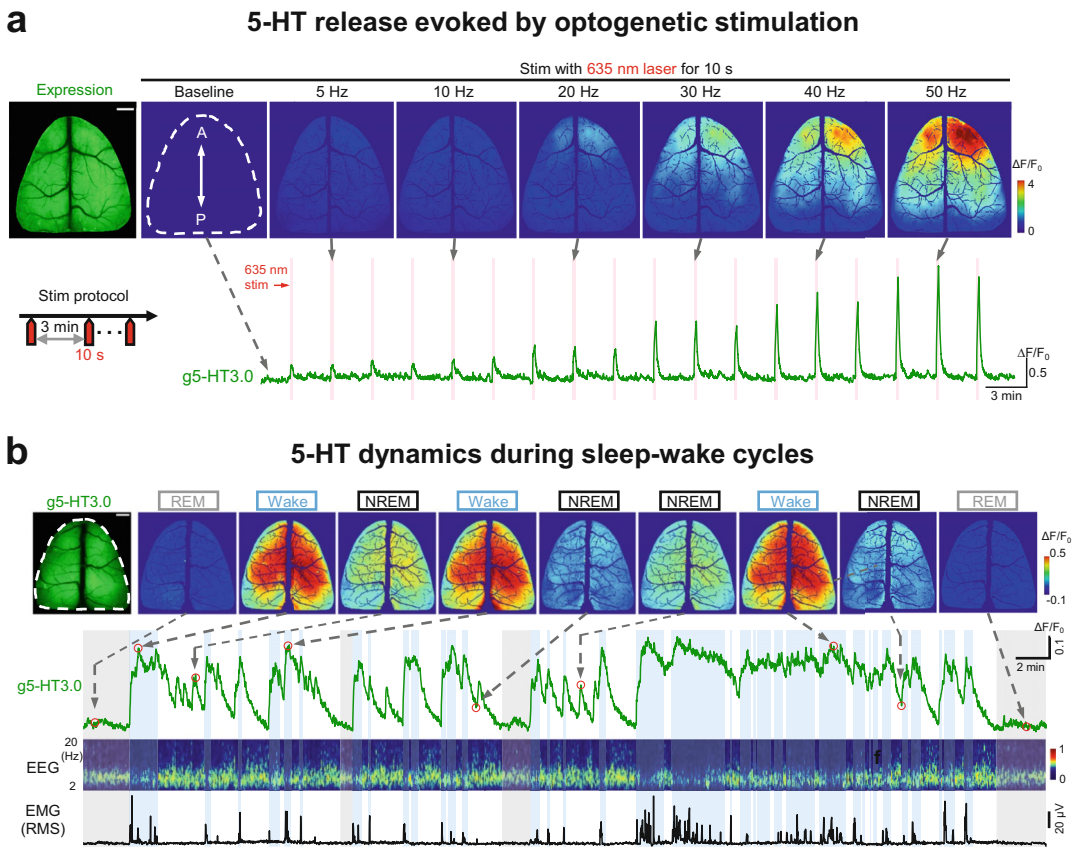

Fig. 6 Mesoscopic imaging of spatiotemporal 5-HT release in mouse dorsal cortex. (**a**) Example images showing the g5-HT3.0 expression and response (top); representative traces of averaged g5-HT3.0 fluorescence changes in the dorsal cortex (bottom). The dashed white outline indicates the ROI for traces analysis. Scale bar, 1 mm. (**b**) Representative fluorescence image of g5-HT3.0 and pseudocolor images of fluorescence changes during sleep–wake cycles (top); representative traces of averaged g5-HT3.0 signals, EEG and EMG signals. (Adapted from Deng et al. [50])

window for imaging most of the dorsal cortex. Finally, EEG/EMG electrodes were implanted for EEG/EMG recording and a metal chamber was affixed to the skull surface. After a week of recovery and habituation to head-fixed conditions, the third step experiments were implemented, including mesoscopic imaging of 5-HT release evoked by optogenetic stimulation and during sleep–wake cycles.

Activation of DRN serotonergic neurons elicited robust g5-HT3.0 signal across the dorsal neocortex and it exhibited a gradient pattern with decreased signals along the anterior-to-posterior axis (Fig. 6a). Meanwhile during the sleep–wake cycle, according to g5-HT3.0 signals, in the mouse dorsal cortex, the 5-HT level was highest during wakefulness and lowest during REM states; and it exhibited obvious oscillations during the NREM sleep

state. In addition, signals in different brain regions were relatively homogenous (Fig. 6b) (*see* **Note 3**). Taken together, these results suggest that the 5-HT release has potential to be spatially heterogenous in the dorsal cortex, which is consistent with the heterogeneity of serotonergic projection density in the cortex [71]. But its release may be globally regulated during the sleep–wake cycle, which leads to relatively homogenous 5-HT release.

5 Notes

1. *Selection of a suitable GPCR scaffold* (In Subheading 2.2)
   It is crucial to choose an appropriate GPCR scaffold for the development of a sensor. If membrane trafficking is not good, sensors tend to remain in the cytosol, which hinders their activation by extracellular ligands and consequently leads to a relatively low response ($\Delta F/F_0$). To address this issue, sensor developers can explore various GPCR scaffolds derived from different subtypes or species. In addition, sensors based on different scaffolds may exhibit distinct responses ($\Delta F/F_0$) and affinities, which can provide the optimal sensor prototype.
2. *Site-directed random mutagenesis* (In Subheading 2.2)
   The site-directed random mutagenesis can be achieved by constructing a library using degenerate primers (e.g. base sequence "NNB" for the mutation site). Considering the existence of 20 different amino acids, it is advisable to screen approximately three times the number of possibilities, resulting in around 60 candidates, which accounts for the random mutations and ensures comprehensive coverage of most possibilities. Alternatively, the library can also be constructed by introducing mutations of 20 different amino acids one by one following PCR transfection for testing in cultured cells [85].
3. *Spatial uniformity of mesoscopic imaging* (In Subheadings 2.3, 3 and 4)
   To better interpret the sensor signals from the entire cortex, it is important to optimize the mesoscopic imaging system to achieve uniform imaging. On the one hand, the sensor should be expressed uniformly. The n-SIM method [62] and the utilization of transgenic mice have shown promise in achieving relatively uniform sensor expression. On the other hand, uniform illumination plays a vital role. The illumination uniformity can be assessed by employing uniform samples such as fluorescent plastic plates or white papers [75].
4. *Spectral unmixing in dual-color mesoscopic imaging* (In Subheading 3)
   For accurate dual-color imaging, it is essential to address the potential bleed-through in spectra. The dual-color imaging

system can employ two independent channels and two sensors with different colors can be sequentially illuminated. Alternatively, if simultaneous imaging of both channels is a priority, two sensors can be excited simultaneously, followed by spectral unmixing in the data processing, such as by linear unmixing [50, 86].

5. *Hemodynamic correction* (In Subheading 3)

   The detected fluorescent signals are not only from ligand concentration-dependent sensor signals but also from other artifacts, particularly those arising from hemodynamics. To evaluate the performance of hemodynamic correction, a negative control can be used, such as membrane-tethered EGFP or a nonbinding mutant sensor, which should show no obvious fluctuations after the application of hemodynamic correction.

6 Summary and Outlook

In this chapter, we have overviewed the principle, development, and properties of GENIs, followed by the application of GENIs with mesoscopic imaging for monitoring NT/NM dynamics, specifically in a case study imaging 5-HT dynamics by the g5-HT3.0 sensor.

Progresses in sensor development will no doubt accelerate the mesoscopic imaging of NTs/NMs with a variety of GENIs. In the future, considering the requirements for mesoscopic imaging, GENIs may be developed and optimized in the following aspects (Fig. 7):

1. Developing more sensors for detecting more NTs/NMs. Based on the understanding of the GENI's principle and the generalizability of sensor developing strategies, a large repertoire of sensors can be developed for detecting more NTs/NMs to expand the toolbox of GENIs.
2. Improving sensitivities of GENIs. For mesoscopic imaging, sensitivity is quite important, especially for detecting NTs/NMs with minor changes. Actually, sensitivities of some GENIs for detecting vital NTs/NMs have been largely improved after iterative optimization, such as GENIs for glutamate [22, 23], DA [33–36], ACh [31, 32], and 5-HT [39, 50].
3. Expanding spectral profiles of GENIs. Most current GENIs are green fluorescent sensors, which precludes multiplexed imaging of multiple neurochemicals simultaneously due to spectral overlap. Some pioneering works have developed red-shifted GENIs, such as R-iGluSnFR1 for glutamate [24], rGRAB$_{DA1m}$, rGRAB$_{DA1h}$, and RdLight1 for DA [34, 36] and

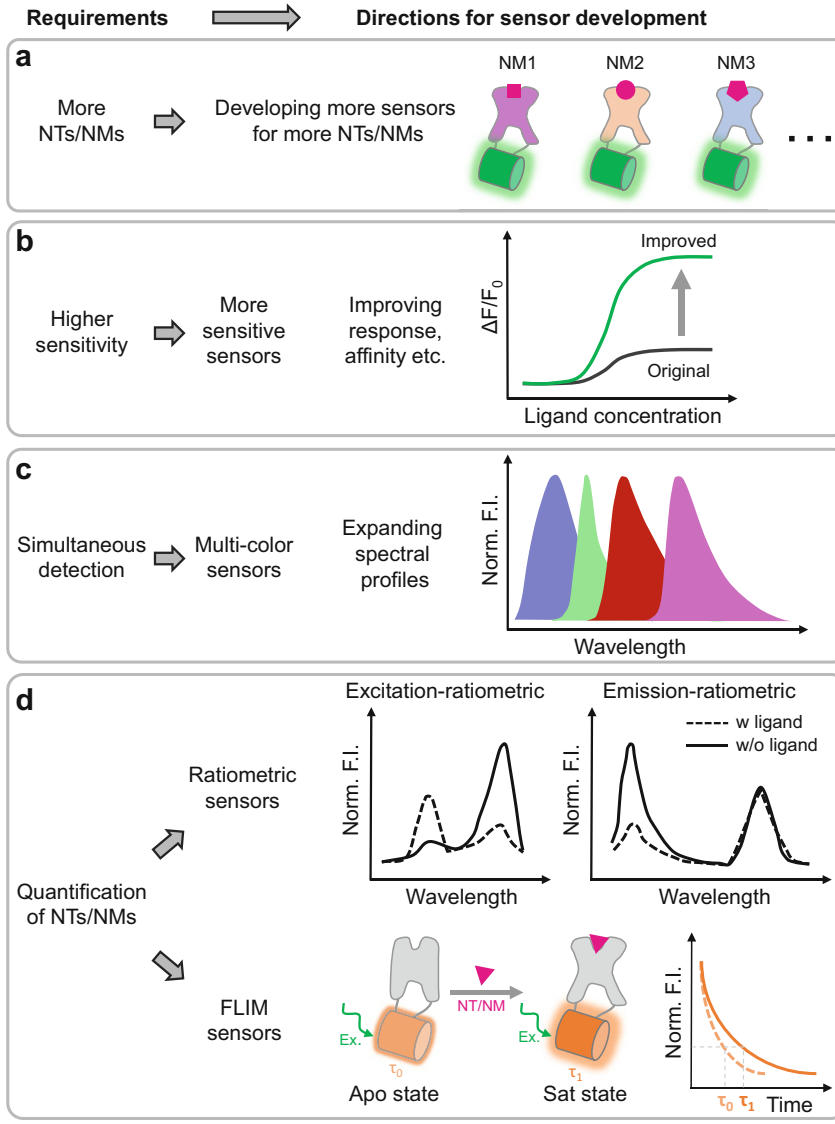

Fig. 7 Future directions for the development of GENIs. Schematic illustrating main directions for further development and optimization of GENIs for four different requirements of mesoscopic imaging. FLIM fluorescence lifetime imaging microscopy

rGRAB$_{5\text{-HT1.0}}$ for 5-HT [50]. Similar strategies can be used to develop red-shifted or even far-red/near-infrared GENIs.

4. Developing GENIs for quantitative imaging. Quantitative imaging is essential for measuring the concentration of NTs/NMs accurately, particularly with changes of tonic level. However, most GENIs are single FP-based and intensiometric. Although they can sensitively report the changes of NT/NM levels, they cannot perform quantitative measurements. At present, there are two kinds of sensors that are capable for

quantitative imaging, including ratiometric sensors and fluorescence lifetime imaging (FLIM)-based sensors. Ratiometric sensors, including excitation-ratiometric and emission-ratiometric sensors, can be excited or emit at distinct wavelengths with or without the ligand binding. Some genetically encoded ratiometric sensors have already been developed, such as some calcium sensors, GEX-GECO1 and GEM-GECO1 [87]. FLIM sensors can report NT/NM levels by fluorescence lifetime instead of fluorescence intensity, which may be ideal sensors for quantification [88], but there are only limited FLIM sensors, largely due to the challenges in sensor development and optimization. Nevertheless, it may be possible to quantitatively measure the dynamics of NTs/NMs in the entire dorsal neocortex by using ratiometric or FLIM GENIs in mesoscopic imaging.

Besides progresses in GENIs, advances in mesoscopic imaging techniques, such as increasing the resolution [89], developing 2-photon/3-photon, or wireless head-mounted mesoscopic imaging systems, will also facilitate the application of GENIs and better understanding of neurotransmission.

References

1. Pereda AE (2014) Electrical synapses and their functional interactions with chemical synapses. Nat Rev Neurosci 15(4):250–263. https://doi.org/10.1038/nrn3708
2. Dong C et al (2022) Fluorescence imaging of neural activity, neurochemical dynamics, and drug-specific receptor conformation with genetically encoded sensors. Annu Rev Neurosci 45(1). https://doi.org/10.1146/annurev-neuro-110520-031137
3. Wu Z, Lin D, Li Y (2022) Pushing the frontiers: tools for monitoring neurotransmitters and neuromodulators. Nat Rev Neurosci 23(5):257–274. https://doi.org/10.1038/s41583-022-00577-6
4. Lovinger DM (2010) Neurotransmitter roles in synaptic modulation, plasticity and learning in the dorsal striatum. Neuropharmacology 58(7):951–961. https://doi.org/10.1016/j.neuropharm.2010.01.008
5. Ma S et al (2018) Dual-transmitter systems regulating arousal, attention, learning and memory. Neurosci Biobehav Rev 85:21–33. https://doi.org/10.1016/j.neubiorev.2017.07.009
6. Lesch KP et al (1996) Association of anxiety-related traits with a polymorphism in the serotonin transporter gene regulatory region. Science 274(5292):1527–1531. https://doi.org/10.1126/science.274.5292.1527
7. Theodore WH, Juhasz C, Savic V, Drevets W (2005) Serotonin, depression, and epilepsy. Epilepsia 46:3–3
8. Li Y et al (2021) Synaptic mechanism underlying serotonin modulation of transition to cocaine addiction. Science 373(6560):1252–1256. https://doi.org/10.1126/science.abi9086
9. Sarter M, Bruno JP, Parikh V (2007) Abnormal neurotransmitter release underlying behavioral and cognitive disorders: toward concepts of dynamic and function-specific dysregulation. Neuropsychopharmacology 32(7):1452–1461. https://doi.org/10.1038/sj.npp.1301285
10. Higley MJ, Picciotto MR (2014) Neuromodulation by acetylcholine: examples from schizophrenia and depression. Curr Opin Neurobiol 29:88–95. https://doi.org/10.1016/j.conb.2014.06.004
11. Nitsch RM (1996) From acetylcholine to amyloid: neurotransmitters and the pathology of Alzheimer's disease. Neurodegeneration 5(4):477–482. https://doi.org/10.1006/neur.1996.0066
12. Lotharius J, Brundin P (2002) Pathogenesis of parkinson's disease: dopamine, vesicles and

α-synuclein. Nat Rev Neurosci 3(12): 932–942. https://doi.org/10.1038/nrn983

13. Wang H, Jing M, Li Y (2018) Lighting up the brain: genetically encoded fluorescent sensors for imaging neurotransmitters and neuromodulators. Curr Opin Neurobiol 50:171–178. https://doi.org/10.1016/j.conb.2018.03.010
14. Sabatini BL, Tian L (2020) Imaging neurotransmitter and neuromodulator dynamics in vivo with genetically encoded indicators. Neuron 108(1):17–32. https://doi.org/10.1016/j.neuron.2020.09.036
15. Brun MA et al (2011) Semisynthesis of fluorescent metabolite sensors on cell surfaces. J Am Chem Soc 133(40):16235–16242. https://doi.org/10.1021/ja206915m
16. Nguyen Q-T et al (2010) An in vivo biosensor for neurotransmitter release and in situ receptor activity. Nat Neurosci 13(1):127–132. https://doi.org/10.1038/nn.2469
17. Barnea G et al (2008) The genetic design of signaling cascades to record receptor activation. Proc Natl Acad Sci 105(1):64–69. https://doi.org/10.1073/pnas.0710487105
18. Cardin JA, Crair MC, Higley MJ (2020) Mesoscopic imaging: shining a wide light on large-scale neural dynamics. Neuron 108(1): 33–43. https://doi.org/10.1016/j.neuron.2020.09.031
19. Wang QX et al (2020) The Allen mouse brain common coordinate framework: a 3D reference atlas. Cell 181(4):936–953.e920. https://doi.org/10.1016/j.cell.2020.04.007
20. Dwyer MA, Hellinga HW (2004) Periplasmic binding proteins: a versatile superfamily for protein engineering. Curr Opin Struct Biol 14(4):495–504. https://doi.org/10.1016/j.sbi.2004.07.004
21. Okumoto S et al (2005) Detection of glutamate release from neurons by genetically encoded surface-displayed FRET nanosensors. Proc Natl Acad Sci 102(24): 8740–8745. https://doi.org/10.1073/pnas.0503274102
22. Marvin JS et al (2013) An optimized fluorescent probe for visualizing glutamate neurotransmission. Nat Methods 10(2):162–170. https://doi.org/10.1038/nmeth.2333
23. Marvin JS et al (2018) Stability, affinity, and chromatic variants of the glutamate sensor iGluSnFR. Nat Methods 15(11):936–939. https://doi.org/10.1038/s41592-018-0171-3
24. Wu JH et al (2018) Genetically encoded glutamate indicators with altered color and topology. ACS Chem Biol 13(7): 1832–1837. https://doi.org/10.1021/acschembio.7b01085
25. Marvin JS et al (2019) A genetically encoded fluorescent sensor for in vivo imaging of GABA. Nat Methods 16(8):763–770. https://doi.org/10.1038/s41592-019-0471-2
26. Lobas MA et al (2019) A genetically encoded single-wavelength sensor for imaging cytosolic and cell surface ATP. Nat Commun 10(1):711. https://doi.org/10.1038/s41467-019-08441-5
27. Borden PM et al (2020) A fast genetically encoded fluorescent sensor for faithful in vivo acetylcholine detection in mice, fish, worms and flies. bioRxiv:2020.2002.2007.939504. https://doi.org/10.1101/2020.02.07.939504
28. Unger EK et al (2020) Directed evolution of a selective and sensitive serotonin sensor via machine learning. Cell 183(7):1986–2002.e1926. https://doi.org/10.1016/j.cell.2020.11.040
29. Rosenbaum DM, Rasmussen SGF, Kobilka BK (2009) The structure and function of G-protein-coupled receptors. Nature 459(7245):356–363. https://doi.org/10.1038/nature08144
30. Latorraca NR, Venkatakrishnan AJ, Dror RO (2017) GPCR dynamics: structures in motion. Chem Rev 117(1):139–155. https://doi.org/10.1021/acs.chemrev.6b00177
31. Jing M et al (2018) A genetically encoded fluorescent acetylcholine indicator for in vitro and in vivo studies. Nat Biotechnol 36(8):726–737. https://doi.org/10.1038/nbt.4184
32. Jing M et al (2020) An optimized acetylcholine sensor for monitoring in vivo cholinergic activity. Nat Methods 17(11):1139–1146. https://doi.org/10.1038/s41592-020-0953-2
33. Sun F et al (2018) A genetically encoded fluorescent sensor enables rapid and specific detection of dopamine in flies, fish, and mice. Cell 174(2):481–496.e419. https://doi.org/10.1016/j.cell.2018.06.042
34. Sun F et al (2020) Next-generation GRAB sensors for monitoring dopaminergic activity in vivo. Nat Methods 17(11):1156–1166. https://doi.org/10.1038/s41592-020-00981-9

35. Patriarchi T et al (2018) Ultrafast neuronal imaging of dopamine dynamics with designed genetically encoded sensors. Science 360(6396):10.1126/science.aat4422
36. Patriarchi T et al (2020) An expanded palette of dopamine sensors for multiplex imaging in vivo. Nat Methods 17(11):1147–1155. https://doi.org/10.1038/s41592-020-0936-3
37. Feng J et al (2019) A genetically encoded fluorescent sensor for rapid and specific in vivo detection of norepinephrine. Neuron 102(4):745–761.e748. https://doi.org/10.1016/j.neuron.2019.02.037
38. Oe Y et al (2020) Distinct temporal integration of noradrenaline signaling by astrocytic second messengers during vigilance. Nat Commun 11(1). https://doi.org/10.1038/s41467-020-14378-x
39. Wan J et al (2021) A genetically encoded sensor for measuring serotonin dynamics. Nat Neurosci 24(5):746–752. https://doi.org/10.1038/s41593-021-00823-7
40. Dong C et al (2021) Psychedelic-inspired drug discovery using an engineered biosensor. Cell 184(10):2779–2792.e2718. https://doi.org/10.1016/j.cell.2021.03.043
41. Kubitschke M et al (2022) Next generation genetically encoded fluorescent sensors for serotonin. Nat Commun 13(1):7525. https://doi.org/10.1038/s41467-022-35200-w
42. Peng WL et al (2020) Regulation of sleep homeostasis mediator adenosine by basal forebrain glutamatergic neurons. Science 369(6508):1208. https://doi.org/10.1126/science.abb0556
43. Wu Z et al (2023) Neuronal activity-induced, equilibrative nucleoside transporter-dependent, somatodendritic adenosine release revealed by a GRAB sensor. Proc Natl Acad Sci 120(14). https://doi.org/10.1073/pnas.2212387120
44. Wu Z et al (2021) A sensitive GRAB sensor for detecting extracellular ATP in vitro and in vivo. Neuron 110:770–782.e775. https://doi.org/10.1016/j.neuron.2021.11.027
45. Dong H et al (2023) Genetically encoded sensors for measuring histamine release both in vitro and in vivo. Neuron 111(10):1564–1576.e1566. https://doi.org/10.1016/j.neuron.2023.02.024
46. Hannon J, Hoyer D (2008) Molecular biology of 5-HT receptors. Behav Brain Res 195(1):198–213. https://doi.org/10.1016/j.bbr.2008.03.020
47. Bunin MA, Wightman RM (1998) Quantitative evaluation of 5-hydroxytryptamine (serotonin) neuronal release and uptake: an investigation of extrasynaptic transmission. J Neurosci 18(13):4854–4860. https://doi.org/10.1523/jneurosci.18-13-04854.1998
48. Thorré K et al (1997) Differential effects of restraint stress on hippocampal 5-HT metabolism and extracellular levels of 5-HT in streptozotocin-diabetic rats. Brain Res 772(1):209–216. https://doi.org/10.1016/S0006-8993(97)00841-X
49. Hashemi P et al (2009) Voltammetric detection of 5-hydroxytryptamine release in the rat brain. Anal Chem 81(22):9462–9471. https://doi.org/10.1021/ac9018846
50. Deng F et al (2024) Improved green and red GRAB sensors for monitoring spatiotemporal serotonin release in vivo. Nat Methods 21(4):692–702. https://doi.org/10.1038/s41592-024-02188-8
51. Kremers G-J, Goedhart J, van Munster EB, Gadella TWJ (2006) Cyan and yellow super fluorescent proteins with improved brightness, protein folding, and FRET Förster radius. Biochemistry 45(21):6570–6580. https://doi.org/10.1021/bi0516273
52. Candelario J, Chachisvilis M (2012) Mechanical stress stimulates conformational changes in 5-hydroxytryptamine receptor 1B in bone cells. Cell Mol Bioeng 5(3):277–286. https://doi.org/10.1007/s12195-012-0232-0
53. Patriarchi T et al (2019) Imaging neuromodulators with high spatiotemporal resolution using genetically encoded indicators. Nat Protoc 14(12):3471–3505. https://doi.org/10.1038/s41596-019-0239-2
54. Bajar BT et al (2016) Improving brightness and photostability of green and red fluorescent proteins for live cell imaging and FRET reporting. Sci Rep-Uk 6(1):20889. https://doi.org/10.1038/srep20889
55. Pédelacq J-D et al (2006) Engineering and characterization of a superfolder green fluorescent protein. Nat Biotechnol 24(1):79–88. https://doi.org/10.1038/nbt1172
56. Kaplitt MG et al (1994) Long-term gene expression and phenotypic correction using adeno-associated virus vectors in the mammalian brain. Nat Genet 8(2):148–154. https://doi.org/10.1038/ng1094-148
57. Wang D, Tai PWL, Gao G (2019) Adeno-associated virus vector as a platform for gene therapy delivery. Nat Rev Drug Discov 18(5):358–378. https://doi.org/10.1038/s41573-019-0012-9

58. Nectow AR, Nestler EJ (2020) Viral tools for neuroscience. Nat Rev Neurosci 21(12): 669–681. https://doi.org/10.1038/s41583-020-00382-z
59. Chan KY et al (2017) Engineered AAVs for efficient noninvasive gene delivery to the central and peripheral nervous systems. Nat Neurosci 20(8):1172–1179. https://doi.org/10.1038/nn.4593
60. Michelson NJ, Vanni MP, Murphy TH (2019) Comparison between transgenic and AAV-PHP.eB-mediated expression of GCaMP6s using in vivo wide-field functional imaging of brain activity. Neurophotonics 6(2):ARTN 025014. https://doi.org/10.1117/1.NPh.6.2.025014
61. Foust KD et al (2009) Intravascular AAV9 preferentially targets neonatal neurons and adult astrocytes. Nat Biotechnol 27(1): 59–65. https://doi.org/10.1038/nbt.1515
62. Hamodi AS et al (2020) Transverse sinus injections drive robust whole-brain expression of transgenes. Elife 9:ARTN e53639. https://doi.org/10.7554/eLife.53639
63. Lohani S et al (2022) Spatiotemporally heterogeneous coordination of cholinergic and neocortical activity. Nat Neurosci 25(12): 1706–1713. https://doi.org/10.1038/s41593-022-01202-6
64. Madisen L et al (2015) Transgenic mice for intersectional targeting of neural sensors and effectors with high specificity and performance. Neuron 85(5):942–958. https://doi.org/10.1016/j.neuron.2015.02.022
65. Xie YC et al (2016) Resolution of high-frequency mesoscale intracortical maps using the genetically encoded glutamate sensor iGluSnFR. J Neurosci 36(4):1261–1272. https://doi.org/10.1523/Jneurosci.2744-15.2016
66. El Marjou F, Jouhanneau C, Krndija D (2021) Targeted transgenic mice using CRISPR/Cas9 technology. In: Ancelin K, Borensztein M (eds) Epigenetic reprogramming during mouse embryogenesis: methods and protocols. Springer US, New York, pp 125–141
67. Dong A et al (2021) A fluorescent sensor for spatiotemporally resolved imaging of endocannabinoid dynamics in vivo. Nat Biotechnol:787–798. https://doi.org/10.1038/s41587-021-01074-4
68. Feng J et al (2024) Monitoring norepinephrine release in vivo using next-generation $GRAB_{NE}$ sensors. Neuron 112:1930–1942.e6. https://doi.org/10.1016/j.neuron.2024.03.001
69. Labouesse MA, Patriarchi T (2021) A versatile GPCR toolkit to track in vivo neuromodulation: not a one-size-fits-all sensor. Neuropsychopharmacology 46(12): 2043–2047. https://doi.org/10.1038/s41386-021-00982-y
70. Soreq H, Seidman S (2001) Acetylcholinesterase – new roles for an old actor. Nat Rev Neurosci 2(4):294–302. https://doi.org/10.1038/35067589
71. Oh SW et al (2014) A mesoscale connectome of the mouse brain. Nature 508(7495): 207–214. https://doi.org/10.1038/nature13186
72. Rynes ML et al (2021) Miniaturized head-mounted microscope for whole-cortex mesoscale imaging in freely behaving mice. Nat Methods 18(4):417–425. https://doi.org/10.1038/s41592-021-01104-8
73. Ma Y et al (2016) Wide-field optical mapping of neural activity and brain haemodynamics: considerations and novel approaches. Philos Trans R Soc B: Biol Sci 371(1705): 20150360. https://doi.org/10.1098/rstb.2015.0360
74. Valley MT et al (2020) Separation of hemodynamic signals from GCaMP fluorescence measured with wide-field imaging. J Neurophysiol 123(1):356–366. https://doi.org/10.1152/jn.00304.2019
75. Couto J et al (2021) Chronic, cortex-wide imaging of specific cell populations during behavior. Nat Protoc 16:3241–3263. https://doi.org/10.1038/s41596-021-00527-z
76. Berger M, Gray JA, Roth BL (2009) The expanded biology of serotonin. Annu Rev Med 60:355–366. https://doi.org/10.1146/annurev.med.60.042307.110802
77. Li Y et al (2016) Serotonin neurons in the dorsal raphe nucleus encode reward signals. Nat Commun 7:10503. https://doi.org/10.1038/ncomms10503
78. Portas CM et al (1998) On-line detection of extracellular levels of serotonin in dorsal raphe nucleus and frontal cortex over the sleep/wake cycle in the freely moving rat. Neuroscience 83(3):807–814. https://doi.org/10.1016/S0306-4522(97)00438-7
79. Ferezou I et al (2007) Spatiotemporal dynamics of cortical sensorimotor integration in behaving mice. Neuron 56(5):907–923. https://doi.org/10.1016/j.neuron.2007.10.007
80. Vanni MP, Murphy TH (2014) Mesoscale transcranial spontaneous activity mapping in GCaMP3 transgenic mice reveals extensive

reciprocal connections between areas of Somatomotor cortex. J Neurosci 34(48): 15931–15946. https://doi.org/10.1523/jneurosci.1818-14.2014

81. Ishimura K et al (1988) Quantitative analysis of the distribution of serotonin-immunoreactive cell bodies in the mouse brain. Neurosci Lett 91(3):265–270. https://doi.org/10.1016/0304-3940(88)90691-X
82. Klapoetke NC et al (2014) Independent optical excitation of distinct neural populations. Nat Methods 11(3):338–346. https://doi.org/10.1038/nmeth.2836
83. Zhuang X et al (2005) Targeted gene expression in dopamine and serotonin neurons of the mouse brain. J Neurosci Methods 143(1):27–32. https://doi.org/10.1016/j.jneumeth.2004.09.020
84. Xu M et al (2015) Basal forebrain circuit for sleep-wake control. Nat Neurosci 18(11): 1641–1647. https://doi.org/10.1038/nn.4143
85. Villette V et al (2019) Ultrafast two-photon imaging of a high-gain voltage indicator in awake behaving mice. Cell 179(7): 1590–1608.e1523. https://doi.org/10.1016/j.cell.2019.11.004
86. Zimmermann T (2005) Spectral imaging and linear unmixing in light microscopy. Adv Biochem Eng Biotechnol 95:245–265. https://doi.org/10.1007/b102216
87. Zhao Y et al (2011) An expanded palette of genetically encoded Ca2+ indicators. Science 333(6051):1888–1891. https://doi.org/10.1126/science.1208592
88. Suhling K et al (2015) Fluorescence lifetime imaging (FLIM): basic concepts and some recent developments. Med Photonics 27:3–40. https://doi.org/10.1016/j.medpho.2014.12.001
89. Fan J et al (2019) Video-rate imaging of biological dynamics at centimetre scale and micrometre resolution. Nat Photonics 13(11):809–816. https://doi.org/10.1038/s41566-019-0474-7
90. Aggarwal A et al (2023) Glutamate indicators with improved activation kinetics and localization for imaging synaptic transmission. Nat Methods 20(6):925–934. https://doi.org/10.1038/s41592-023-01863-6
91. Helassa N et al (2018) Ultrafast glutamate sensors resolve high-frequency release at Schaffer collateral synapses. Proc Natl Acad Sci 115(21):5594–5599. https://doi.org/10.1073/pnas.1720648115
92. Nakamoto C et al (2021) A novel red fluorescence dopamine biosensor selectively detects dopamine in the presence of norepinephrine in vitro. Mol Brain 14(1):173. https://doi.org/10.1186/s13041-021-00882-8
93. Sheu S-H et al (2022) A serotonergic axon-cilium synapse drives nuclear signaling to alter chromatin accessibility. Cell 185(18): 3390–3407.e3318. https://doi.org/10.1016/j.cell.2022.07.026
94. Kitajima N et al (2020) Real-time in vivo imaging of extracellular ATP in the brain with a hybrid-type fluorescent sensor. elife 9. https://doi.org/10.7554/elife.57544
95. Abraham AD et al (2021) Release of endogenous dynorphin opioids in the prefrontal cortex disrupts cognition. Neuropsychopharmacology 46(13): 2330–2339. https://doi.org/10.1038/s41386-021-01168-2
96. Melzer S et al (2021) Bombesin-like peptide recruits disinhibitory cortical circuits and enhances fear memories. Cell 184(22): 5622–5634.e5625. https://doi.org/10.1016/j.cell.2021.09.013
97. Kroning KE, Wang W (2021) Designing a single protein-chain reporter for opioid detection at cellular resolution. Angew Chem Int Ed 60(24):13358–13365. https://doi.org/10.1002/anie.202101262
98. Duffet L et al (2022) A genetically encoded sensor for in vivo imaging of orexin neuropeptides. Nat Methods 19(2):231–241. https://doi.org/10.1038/s41592-021-01390-2
99. Ino D, Tanaka Y, Hibino H, Nishiyama M (2022) A fluorescent sensor for real-time measurement of extracellular oxytocin dynamics in the brain. Nat Methods 19(10): 1286–1294. https://doi.org/10.1038/s41592-022-01597-x
100. Qian T et al (2023) A genetically encoded sensor measures temporal oxytocin release from different neuronal compartments. Nat Biotechnol. https://doi.org/10.1038/s41587-022-01561-2
101. Wang H et al (2023) A tool kit of highly selective and sensitive genetically encoded neuropeptide sensors. Science 382(6672): eabq8173. https://doi.org/10.1126/science.abq8173
102. Duffet L et al (2023) Optical tools for visualizing and controlling human GLP-1 receptor activation with high spatiotemporal resolution. elife 12:RP86628. https://doi.org/10.7554/eLife.86628